COMMUNICATIONS IN COMPUTATIONAL PHYSICS
Vol. **5**, No. 1, pp. 126-141

Commun. Comput. Phys.
January 2009

A Hybrid Finite Element-Laplace Transform Method for the Analysis of Transient Electromagnetic Scattering by an Over-Filled Cavity in the Ground Plane

Junqi Huang, Aihua W. Wood* and Michael J. Havrilla

Air Force Institute of Technology, 2950 Hobson Way, Wright-Patterson AFB, OH 45433, USA.

Received 29 November 2007; Accepted (in revised version) 1 May 2008

Communicated by Gang Bao

Available online 15 July 2008

Abstract. A hybrid finite element-Laplace transform method is implemented to analyze the time domain electromagnetic scattering induced by a 2-D overfilled cavity embedded in the infinite ground plane. The algorithm divides the whole scattering domain into two, interior and exterior, sub-domains. In the interior sub-domain which covers the cavity, the problem is solved via the finite element method. The problem is solved analytically in the exterior sub-domain which slightly overlaps the interior sub-domain and extends to the rest of the upper half plane. The use of the Laplace transform leads to an analytical link condition between the overlapping sub-domains. The analytical link guides the selection of the overlapping zone and eliminates the need to use the conventional Schwartz iteration. This dramatically improves the efficiency for solving transient scattering problems. Numerical solutions are tested favorably against analytical ones for a canonical geometry. The perfect link over the artificial boundary between the finite element approximation in the interior and analytical solution in the exterior further indicates the reliability of the method. An error analysis is also performed.

AMS subject classifications: 35M10, 65M60

Key words: Overfilled cavity, time domain electromagnetic scattering, Laplace transform, finite element method.

1 Introduction

In the last decades, the time-domain finite element method (TDFEM) has evolved into a powerful numerical tool making it possible to solve a variety of complicated electromagnetic problems (see, e.g., [1–9]). The TDFEM applied to scattering by cavities are reported

*Corresponding author. *Email addresses:* Junqi.Huang@afit.edu (J. Huang), Aihua.Wood@afit.edu (A. W. Wood), Michael.Havrilla@afit.edu (M. J. Havrilla)

in [10–15]. It is well known that TDFEM is relatively time consuming since it needs to solve a linear system at each time step. Others have attacked the transient scattering problems with integral equations techniques [16], and series representation approach [17]. Recently, the domain decomposition (DD) method has emerged as a promising technique supplementing the TDFEM [18–20]. The DD method typically partitions the simulated area into a number of sub-domains and Lagrange multipliers are used to enforce the interface continuity condition. Traditionally, the DD method calls for the iterative matching of the link condition (Schwartz link [21]), which incurs significant computational expense.

In [22], we solve the scattering problem in the frequency domain using a hybrid boundary integral - finite element method (BI-FEM) (see, also, [23, 24] and the references therein for this hybrid method). In this technique, an artificial boundary, typically a semi-circle, is placed over the cavity and the interior numerical solution is matched with the exterior analytical solution via the introduction of a boundary operator. The boundary operator gives rise to a non-standard boundary condition on the semi-circle which demands the implementation of a boundary array. An additional hurdle associated with the hybrid method in solving time domain problems stems from the convolution operation. The time-dependency of the artificial boundary requires the storage of historic contributions of the field.

In this paper, the DD technique is integrated into the BI-FEM. In this hybrid approach, the computational domain is partitioned into two sub-domains such that the interior problem is solved numerically and exterior analytically. Specifically, we incorporate three techniques to solve the time domain scattering problem: 1) The hybrid BI-FEM method, in which an analytical solution defined in the exterior domain is used to match the boundary condition of the interior numerical model; 2) DD method, where the whole domain is divided into two sub-domains and the link condition over the overlapped zone between the interior and exterior domains is matched; 3) The Laplace transform (LT) method, here a time dependent kernel function is obtained enabling the explicit evaluation of the boundary condition and thus avoiding the expensive Schwartz iteration. Our algorithm is implemented using the *pdetool* under the GUI environment of Matlab. We developed an analytical solution for a canonical model and compared it against our numerical results. We also plotted the linkage between the exterior analytical solution and the interior numerical one. The overall good agreement between analytical and numerical solutions gives confidence of the reliability of our fast algorithm. The accuracy of our method is further demonstrated by a mesh size related error analysis.

2 Problem setting

Mathematical treatment of time harmonic electromagnetic scattering from cavities are reported in [25] for over-filled cavities, and [26–28] for non-protruding cavities. A detailed mathematical description of the variational method for transient electromagnetic

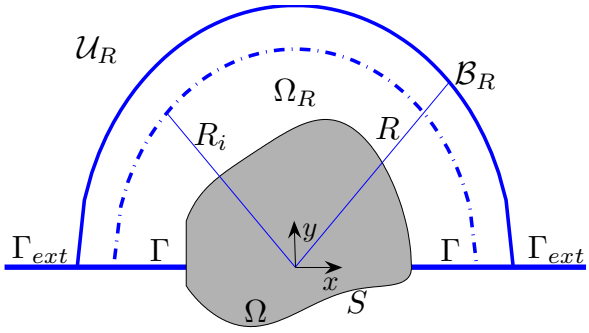

Figure 1: Cavity geometry.

scattering of 2-D overfilled cavities embedded in an infinite ground plane is provided in [29]. Here we highlight the necessary formulations for completeness. The cavity geometry is depicted in Fig. 1, where Ω is the cross section of a z-invariant cavity in the infinite ground plane such that its fillings of relative permittivity $\epsilon_r \neq 1$ protrudes above the ground plane, S the cavity wall, $\mathcal{B}_R$ the semi-disk with radius R large enough to completely enclose the overfilled portion of the cavity, Γ the portion of the ground plane inside $\mathcal{B}_R$, Γ_{ext} the infinite ground plane outside $\mathcal{B}_R$, Ω_R the region consisting of the cavity Ω and the homogeneous part between $\mathcal{B}_R$ and Γ. In addition, R_i is a radius slightly less than R, such that $\mathcal{B}_{R_i}$ still completely encloses the cavity, and finally, $\mathcal{U}_{R_i}$ the exterior to $\mathcal{B}_{R_i}$ overlapping Ω_R by a semi-circular band of width $R-R_i$: $\mathcal{U}_{R_i}=\{(r,\theta):r>R_i,0<\theta<\pi\}$.

2.1 TM^z polarization

As in [22], the scattered field u^s satisfies the following exterior problem:

$$-\Delta u^s+\frac{\partial^2 u^s}{\partial t^2}=0 \quad \text{in } \mathcal{U}_{R_i}, \tag{2.1}$$

$$u^s=u^s_{R_i} \quad \text{on } \sqrt{x^2+y^2}=R_i, \tag{2.2}$$

$$u^s=0 \quad \text{on } y=0,\ |x|\geq R_i, \tag{2.3}$$

$$u^s=\partial u^s/\partial t=0 \quad \text{at } t=0, \tag{2.4}$$

and the radiation condition:

$$\lim_{r\to\infty}\sqrt{r}\left(\frac{\partial u^s}{\partial r}+\frac{\partial u^s}{\partial t}\right)=0. \tag{2.5}$$

We shall use LM, light meter, for the time unit. Taking the Laplace transform $\{t\to p\}$, Eq. (2.1) subject to the initial conditions (2.4) becomes:

$$-\Delta\bar{u}^s+p^2\bar{u}^s=0 \quad \text{in } \mathcal{U}_{R_i}, \tag{2.6}$$

where $\bar{u}^s$ is the transform of u^s.

In polar coordinates, the Helmholtz equation (2.6) becomes

$$\frac{\partial^2 \bar{u}^s}{\partial r^2}+\frac{1}{r}\frac{\partial \bar{u}^s}{\partial r}+\frac{1}{r^2}\frac{\partial^2 \bar{u}^s}{\partial \theta^2}-p^2\bar{u}^s=0. \tag{2.7}$$

We then have the solution of Eq. (2.7) subject to boundary conditions (2.2)-(2.3) and radiation condition (2.5)

$$\bar{u}^s(r,\theta,p)=\frac{2}{\pi}\sum_{n=1}^{\infty}\left(\frac{K_n(pr)}{K_n(pR_i)}\int_0^{\pi}\bar{u}^s_{R_i}(\varphi,p)\sin(n\varphi)d\varphi\right)\sin(n\theta), \tag{2.8}$$

where $K_n(\cdot)$ is the n^{th}-order modified Bessel function of the second kind. On B_R, we have

$$\bar{u}^s(R,\theta,p)=\frac{2}{\pi}\sum_{n=1}^{\infty}\left(\frac{K_n(pR)}{K_n(pR_i)}\int_0^{\pi}\bar{u}^s_{R_i}(\varphi,p)\sin(n\varphi)d\varphi\right)\sin(n\theta). \tag{2.9}$$

Letting

$$\mathcal{K}_n(t)=L^{-1}\left[\frac{K_n(pR)}{K_n(pR_i)}\right],$$

where L^{-1} indicates the inverse laplace transform, we obtain the time domain scattered field on B_R as

$$u^s(R,\theta,t)=\frac{2}{\pi}\sum_{n=1}^{\infty}\left(\int_0^{\pi}\mathcal{K}_n(t)*u^s_{R_i}(\varphi,t)\sin(n\varphi)d\varphi\right)\sin(n\theta). \tag{2.10}$$

Eq. (2.10) provides a link condition between the exterior problem and the following interior problem for the total field:

$$-\Delta u+\epsilon_r\frac{\partial^2 u}{\partial t^2}=0 \quad \text{in } \Omega_R, \tag{2.11}$$

$$u=u_R \quad \text{on } \mathcal{B}_R, \tag{2.12}$$

$$u=0 \quad \text{on } \Gamma\cup S, \tag{2.13}$$

$$u=0;\quad \partial u/\partial t=u_{t0} \quad \text{at } t=0, \tag{2.14}$$

where

$$u_R=u^s(x,y)+u^i(x,y)+u^r(x,y),\quad x,y\in\mathcal{B}_R, \tag{2.15}$$

u^i and u^r are the incident and reflected fields respectively.

Using the general second-order difference scheme, Eqs. (2.11)-(2.14) may be written as:

$$-\Delta u^{m+1}+\frac{\epsilon_r}{\delta t^2}u^{m+1}=\frac{\epsilon_r}{\delta t^2}(2u^m-u^{m-1}) \quad \text{in } \Omega_R, \tag{2.16}$$

$$u^{m+1}=u_R^{m+1} \quad \text{on } \mathcal{B}_R, \tag{2.17}$$

$$u^{m+1}=0 \quad \text{on } \Gamma\cup S, \tag{2.18}$$

$$u^{-1}=0;\quad u^0=\delta t\,u_{t0}, \tag{2.19}$$

where m is the time step index ($m=0,1,2,\cdots$) and δt the time step size.

With *pdetool* under GUI environment of Matlab, Eq. (2.16), classified as an elliptic equation subject to the Dirichlet boundary conditions (2.17) and (2.18) can then be solved by calling the function

$$u=assempde(b,p,e,t,c,a,f),$$

where b describes the boundary condition, p,e and t specify the mesh grid, and c,a, and f are the coefficients in the governing equation. Specifically, $c=1$, $a=\epsilon_r/\delta t^2$, and $f=a(2u^m-u^{m-1})$.

2.2 TE^z Polarization

In this case, the scattered field u^s satisfies the following exterior problem:

$$-\Delta u^s+\frac{\partial^2 u^s}{\partial t^2}=0 \quad \text{in } \mathcal{U}_{R_i}, \tag{2.20}$$

$$u^s=u^s_{R_i} \quad \text{on } \sqrt{x^2+y^2}=R_i, \tag{2.21}$$

$$\partial u^s/\partial n=0 \quad \text{on } y=0,\ |x|\geq R_i, \tag{2.22}$$

$$u^s=\partial u^s/\partial t=0 \quad \text{at } t=0 \tag{2.23}$$

and the radiation condition (2.5). As in the TM case, we first rewrite the differential equation in polar form and solve the problem in the Laplace transform domain. We then take the inverse transform on B_R and obtain the solution to the exterior problem evaluated at $r=R$ to be:

$$u^s(R,\theta,t)=\frac{2}{\pi}\sum_{n=0}^{\infty}\delta_n\left(\int_0^{\pi}\mathcal{K}_n(t)*u^s_{R_i}(\varphi,t)\cos(n\varphi)d\varphi\right)\cos(n\theta), \tag{2.24}$$

where

$$\delta_n=\begin{cases}1/2 & n=0,\\ 1 & n>0.\end{cases} \tag{2.25}$$

Similarly, Eq. (2.24) provides a link condition for the interior problem for the total field:

$$-\nabla\cdot(\epsilon_r^{-1}\nabla u)+\frac{\partial^2 u}{\partial t^2}=0 \quad \text{in } \Omega_R, \tag{2.26}$$

$$u=u_R \quad \text{on } \mathcal{B}_R, \tag{2.27}$$

$$\partial u/\partial n=0 \quad \text{on } \Gamma\cup S, \tag{2.28}$$

$$u=0;\quad \partial u/\partial t=u_{t0} \quad \text{at } t=0, \tag{2.29}$$

where u_R is as in Eq. (2.15).

Similar to the TM case, we can solve the problem by directly calling the function $u=assempde(b,p,e,t,c,a,f)$. Here, b describes the mixed boundary condition with Neumann condition on the cavity wall and Dirichlet condition on the half-cylinder which is calculated using the exterior problem. In this case, the values of c,a, and f are the same as those given in the TM case except here we have $\epsilon_r=1$.

3 Numerical evaluation

3.1 Overlapping zone

In order to solve the discrete system (2.26)-(2.29), u_R must be known. The field u_R can be evaluated via Eq. (2.15) where u^s is calculated by the formula (2.10) for TM and (2.24) for TE respectively. In turn, (2.10) and (2.24) depend on the values of u^s on R_i which are defined on the interior nodes of problem (2.26)-(2.29). Hence this appears to be a recursive procedure. The coupling relationship between the overlapped domains is usually solved via the so-called Schwartz iteration [21]. The basis of the scheme is to alternatively solve the inner and outer problems by updating the link condition until the convergence criterion is satisfied. However, as can be seen below, the time-consuming Schwartz iteration may be avoided by appropriately choosing the overlapped region and time step size. This is possible due to the special characteristics of wave propagation in the time domain.

Based on the convolution principle, the time dependent terms contained in Eqs. (2.10) and (2.24) can be rewritten as:

$$\mathcal{K}_n(t)*u^s_{R_i}(\varphi,t)=\int_0^t \mathcal{K}_n(t-\tau)u^s_{R_i}(\varphi,\tau)d\tau. \tag{3.1}$$

Here, $\mathcal{K}_n(t)$ can be numerically inverted from the Laplace domain using techniques developed in [30] and [31] assuming it is smooth enough in the interested domain. Unfortunately, $\mathcal{K}_n(t)$ has a singularity at $t=0$ as can be seen using the asymptotic expansion of the Bessel function as $p\to\infty$. The singularity can not be treated appropriately with the numerical inversion scheme. In fact, direct numerical inversion of $\mathcal{K}_n(t)$ only gives a satisfactory result for $t>t_{min}$ (numerical test indicates that $t_{min}\simeq 10^{-4}$). To overcome this hurdle, we rewrite Eq. (3.1) via integration by parts as

$$\mathcal{K}_n(t)*u^s_{R_i}(\varphi,t)=\int_0^t \mathcal{K}^*(t-\tau)\dot{u}^s_{R_i}(\varphi,\tau)d\tau, \tag{3.2}$$

where

$$\mathcal{K}^*_n(t)=L^{-1}\left[\frac{1}{p}\frac{K_n(pR)}{K_n(pR_i)}\right],\quad \dot{u}^s_{R_i}=\frac{\partial}{\partial t}u^s_{R_i}(\varphi,t).$$

It can be verified that $\mathcal{K}^*_n(t)$ has no singularity and can be written as

$$\mathcal{K}^*_n(t)=L^{-1}\left[\frac{1}{p}\frac{K_n(pR)}{K_n(pR_i)}\right]=L^{-1}\left[\frac{1}{p}\frac{K^*_n(pR)e^{-pR}}{K^*_n(pR_i)e^{-pR_i}}\right],$$

or

$$\mathcal{K}^*_n(t)=L^{-1}\left[\frac{1}{p}\frac{K^*_n(pR)}{K^*_n(pR_i)}e^{-p(R-R_i)}\right],$$

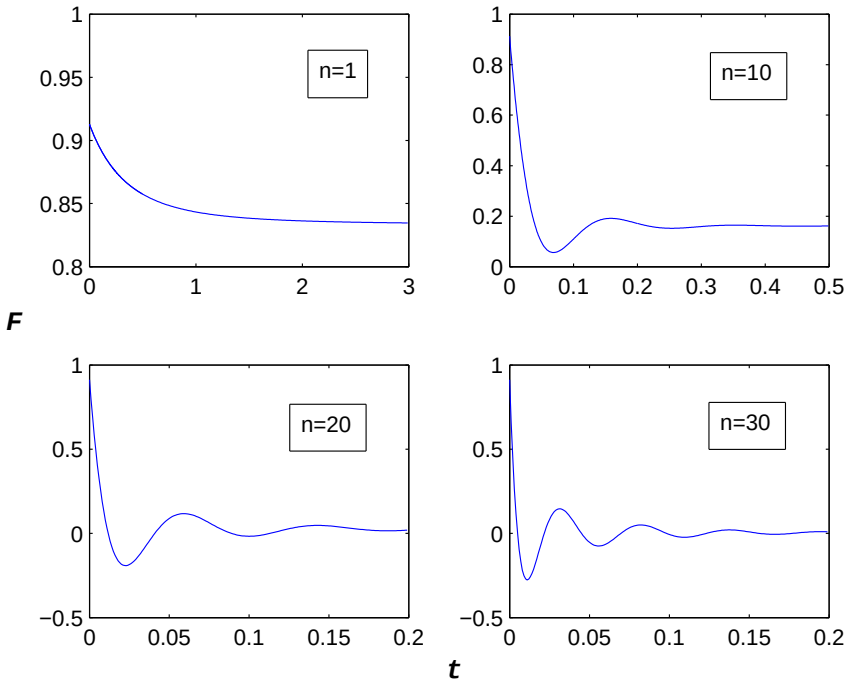

Figure 2: Characteristics of $\mathcal{F}_n(t)$.

where $K_n^*(z)$ is the scaled part of Bessel function $K_n(z)$ by the factor e^z (see [32, 33]). Letting

$$\mathcal{F}_n(t) = L^{-1}\left[\frac{1}{p}\frac{K_n^*(pR)}{K_n^*(pR_i)}\right]$$

and employing the delay property of the Laplace transform, $\mathcal{K}_n(t)^*$ can be written as

$$\mathcal{K}_n^*(t) = \mathcal{F}_n[t-(R-R_i)].$$

This reveals that there is a propagation delay $\Delta = R - R_i$ on the boundary $r = R$ in response to the disturbance that originated at $r = R_i$. Separating the factor of delay enables us to rewrite Eq. (3.2) as

$$\mathcal{K}_n(t) * u_{R_i}^s(\varphi,t) = \int_0^{t-\Delta} \mathcal{F}_n(t-\Delta-\tau)\dot{u}_{R_i}^s(\varphi,\tau)d\tau. \tag{3.3}$$

Obviously, if $\Delta \geq \delta t$, the integral in Eq. (3.3) will not involve the value of $u_{R_i}^s$ at the current time step, rendering iteration unnecessary. In other words, if the overlapped domain, $(R_i \leq r \leq R)$, has a larger span than the distance traveled by the wave cell from $r = R_i$ over a single time step, the Schwartz iteration can be avoided. The boundary condition on $r = R$ calls for just the data of those wave cells sent before $t - \Delta$. Consequently, the evaluations of (2.10) and (2.24) are explicit. As an example, say $\Delta = \delta t$, and k_c is the current time step

index. The values of $u^s_{R_i}$ at $t=0,\delta t,2\delta t,3\delta t,\cdots,(k_c-1)\delta t$ are already available and can be used to evaluate the integral in Eq. (3.3). Clearly, judicious choices of the overlapping domain and time step size are critical in time efficiency.

3.2 Boundary integral

The smoothness of the function $\mathcal{F}_n(t)$ is demonstrated in Fig. 2 for selected n, the order of the Bessel function. It is observed that the oscillation of $\mathcal{F}_n(t)$ increases with n. Note, the function $\mathcal{F}_n(t)$ can be preliminarily obtained by numerically inverting its image function and saving the data for further use since it only depends on R_i and R.

Denote $\Delta=m\delta t,m\geq 1$. The current value of $u^s_{R_i}(\varphi,t)$ in Eq. (3.3) can be evaluated using the interpolation scheme based on the first (k_C-m) values already calculated. Specifically, we have

$$u^s_{R_i}(\varphi,t)=\sum_{k=1}^{k_c-m} u^s_{R_i}(\varphi,t_k)N_k(t), \tag{3.4}$$

where $N_k(t)$ is the basis function equaling 1 at $t=t_k$ and zero otherwise.

With the values of $\mathcal{F}_n(t)$ and $u^s_{R_i}(\varphi,t)$ available, Eq. (3.1) can be numerically integrated by simply calling the Matlab built-in function. The linear system (2.26)-(2.29) can then be easily solved by calling the built-in functions of *pdetool*. Once the total field at the current time step is calculated, we update the right hand side vector F_i and G_i to step forward.

3.3 Incident and reflected fields

We assume that the scatterer is illuminated by a Neumann pulse. The incident wave is defined as [34]:

$$u^i(x,y,t)=-\frac{2\eta}{\sigma^2}e^{-\eta^2/\sigma^2}, \tag{3.5}$$

where $\eta=t-t_0+(x-x_0)\cos(\vartheta)+(y-y_0)\sin(\vartheta)$, x_0 and y_0 are the reference coordinates, t_0 the reference time, σ the form factor of the pulse, and ϑ the incident angle. Then the reflected field can be written as:

$$u^r(x,y,t)=\frac{2\mu}{\sigma^2}e^{-\mu^2/\sigma^2} \tag{3.6}$$

for the TM-polarization, and

$$u^r(x,y,t)=-\frac{2\mu}{\sigma^2}e^{-\mu^2/\sigma^2} \tag{3.7}$$

for the TE-polarization, where $\mu=t-t_0+(x-x_0)\cos(\vartheta)+(-y-y_0)\sin(\vartheta)$ is obtained by setting $y=-y$ (image location) in η.

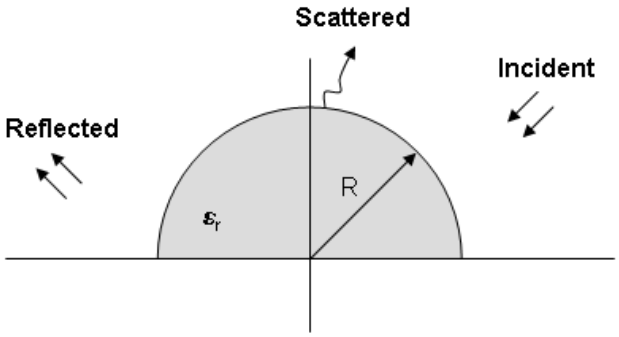

Figure 3: Cross-sectional view of scattering induced by half-cylinder.

4 Validation of the numerical scheme

To test the reliability of the algorithm developed in the paper, we design a special scatterer such that an analytical solution to the scattering problem is possible. In particular, we consider a void cavity consisting entirely of the over-filled portion which takes the form of a half cylinder with cross-sectional dimensions shown in Fig. 3. Based on image theory, this simply indicates scattering from a material cylinder. For this scenario, we set the artificial boundary to coincide with the boundary of the scatterer, the semi-circle. Inside the scatterer, the total field can be found in the Laplace-Fourier domain to be

$$\hat{\hat{u}}(r,n,p) = AI_n(\sqrt{\varepsilon_r}pr); \tag{4.1}$$

while the scattered field outside the scatterer to be

$$\hat{\hat{u}}^s(r,n,p) = BK_n(\sqrt{\varepsilon_r}pr), \tag{4.2}$$

where A and B are constants to be determined by the link conditions over the interface ($r=R$). Here, I_n and K_n are n^{th}-order modified Bessel functions of the first and second kind, respectively. With Neumann incidence, the link criterion is dictated by the following boundary conditions:

$$(\hat{\hat{u}})_{r=R} = \left(\hat{\hat{u}}^s + \hat{\hat{u}}^i + \hat{\hat{u}}^r\right)_{r=R}, \tag{4.3}$$

and

$$\beta\frac{\partial}{\partial r}(\hat{\hat{u}})_{r=R} = \frac{\partial}{\partial r}\left(\hat{\hat{u}}^s + \hat{\hat{u}}^i + \hat{\hat{u}}^r\right)_{r=R}, \tag{4.4}$$

where β=1 for TE-polarization and β=$1/\varepsilon_r$ for TM-polarization. Incorporating the above link conditions, we have, in the Laplace-Fourier domain, the interior total field

$$\hat{\hat{u}}(R,n,p) = \frac{\frac{1}{p}\frac{\partial}{\partial r}(\hat{\hat{u}}^i + \hat{\hat{u}}^r)_R - (\hat{\hat{u}}^i + \hat{\hat{u}}^r)_R \frac{K_n'(pR)}{K_n(pR)}}{\beta\sqrt{\varepsilon_r}\frac{I_n'(\sqrt{\varepsilon_r}pR)}{I_n(\sqrt{\varepsilon_r}pR)} - \frac{K_n'(pR)}{K_n(pR)}} \frac{I_n(\sqrt{\varepsilon_r}pr)}{I_n(\sqrt{\varepsilon_r}pR)}, \tag{4.5}$$

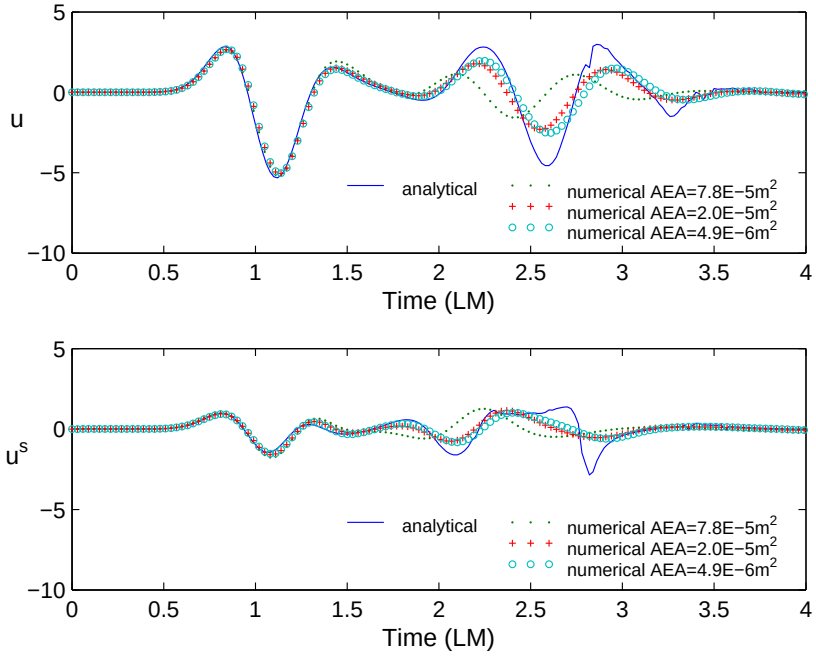

Figure 4: TM solutions: $r=0.2m,\theta=45^o$.

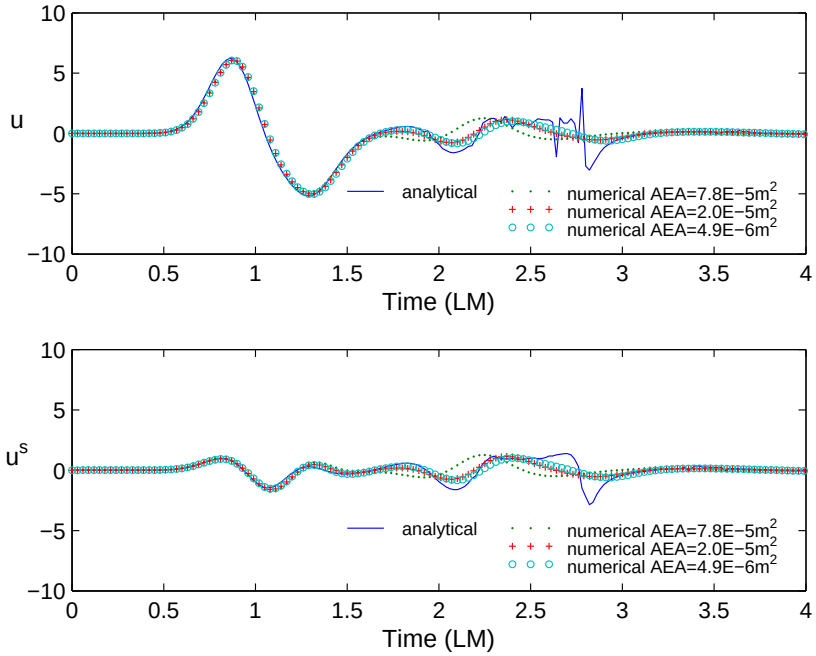

Figure 5: TE solutions: $r=0.2m,\theta=45^o$.

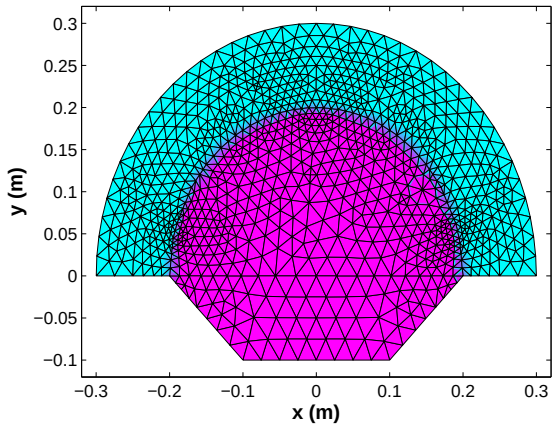

Figure 6: Mesh of interior domain.

and the exterior scattered field

$$\hat{\hat{u}}^s(R,n,p)=\frac{\frac{1}{p}\frac{\partial}{\partial r}(\hat{\hat{u}}^i+\hat{\hat{u}}^r)_R-\beta\sqrt{\varepsilon_r}(\hat{\hat{u}}^i+\hat{\hat{u}}^r)_R\frac{I_n'(\sqrt{\varepsilon_r}pR)}{I_n(\sqrt{\varepsilon_r}pR)}}{\beta\sqrt{\varepsilon_r}\frac{I_n'(\sqrt{\varepsilon_r}pR)}{I_n(\sqrt{\varepsilon_r}pR)}-\frac{K_n'(pR)}{K_n(pR)}}\frac{K_n(pr)}{K_n(pR)}. \tag{4.6}$$

Taking the inverse Fourier transform gives the corresponding fields in the Laplace domain as

$$\bar{u}(r,\theta,p)=\frac{2}{\pi}\sum_{n=1}^{\infty}\hat{u}(r,n,p)\sin(n\theta) \tag{4.7}$$

and

$$\bar{u^s}(r,\theta,p)=\frac{2}{\pi}\sum_{n=1}^{\infty}\hat{\hat{u}}^s(r,n,p)\sin(n\theta) \tag{4.8}$$

for TM polarization, and

$$\bar{u}(r,\theta,p)=\frac{2}{\pi}\sum_{n=0}^{\infty}\delta_n\hat{u}(r,n,p)\cos(n\theta) \tag{4.9}$$

and

$$\bar{u^s}(r,\theta,p)=\frac{2}{\pi}\sum_{n=0}^{\infty}\delta_n\hat{\hat{u}}^s(r,n,p)\cos(n\theta) \tag{4.10}$$

for TE polarization, where δ_n is as defined in (2.25). Eqs. (4.7)-(4.10) can then be evaluated by the numerical inverse algorithm [35].

In Figs. 4 and 5, the numerical solutions are plotted against the corresponding analytical ones for TM and TE polarizations respectively. The late time discrepancy reflects the accumulated effect of the time-marching scheme, mesh size, and especially the convolution calculation, Eq. (3.3). We observe that the error decreases as the average element area (AEA) decreases; the opposite is true as the time step is reduced.

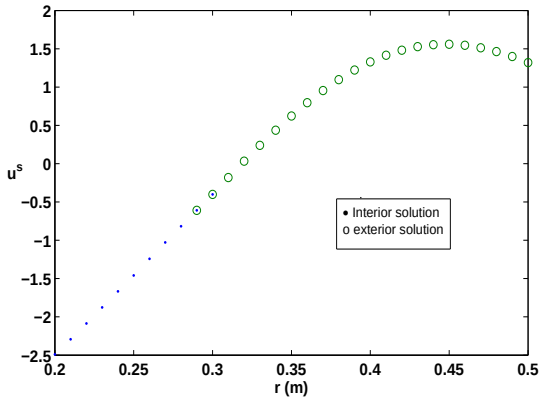

Figure 7: Linkage of TM solutions at $\theta=45^o, t=2.0LM$.

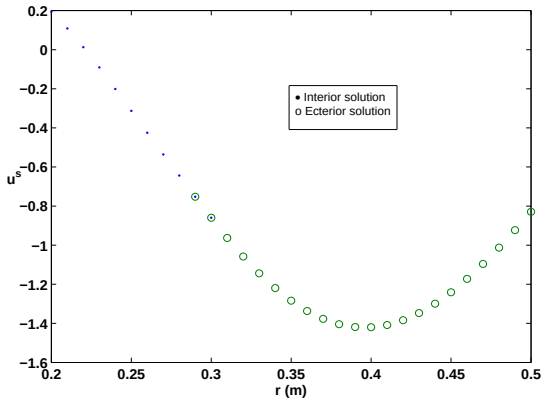

Figure 8: Linkage of TE solutions at $\theta=45^o, t=2.0LM$.

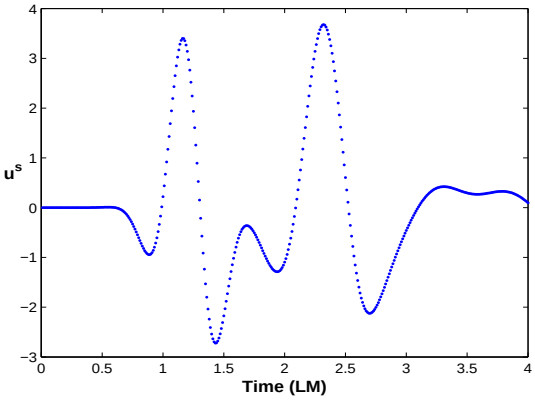

Figure 9: TM scattered field at $r=0.25m, \theta=60^o$.

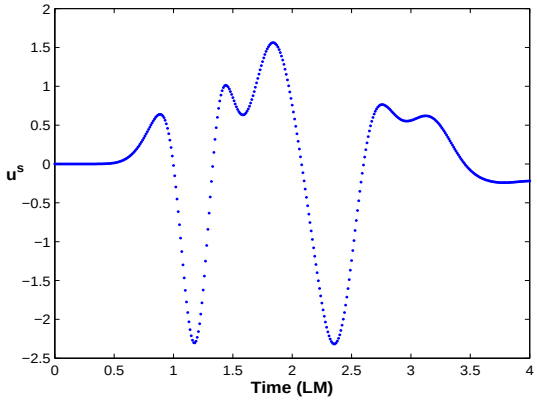

Figure 10: TE scattered field at $r=0.25m, \theta=60^o$.

5 Numerical experiment

Next, we consider a dual-shaped cavity with a 0.4 meter aperture upon the ground plane. The portion below the ground plane is a regular trough of depth 0.1 meter and bottom width 0.2 meter. The boundary of the exterior sub-domain is set at radius $R_i=0.25$ meter, and that of the interior at $R=0.3$ meter. The rest of the values of the problem parameters are given in Table 1. Figs. 7 and 8 show perfect links of the scattered fields between the interior and exterior domains for TM and TE polarizations respectively at an incident angle of $\theta=45^o$ and time $t=2.0(LM)$. The scattered fields for both polarizations are plotted against time at a fixed location, $r=0.25$ meter, $\theta=60^o$, in Figs. 9 and 10.

Table 1: Parameter values used in the simulation.

ε_r	ϑ	t_0	x_0	y_0	σ	δt
4.0	$\pi/4$	0.5	0.5	0.5	0.2	0.01

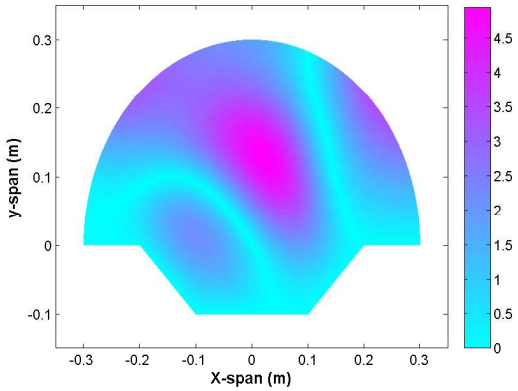

Figure 11: TM total field at $t=2.0LM$.

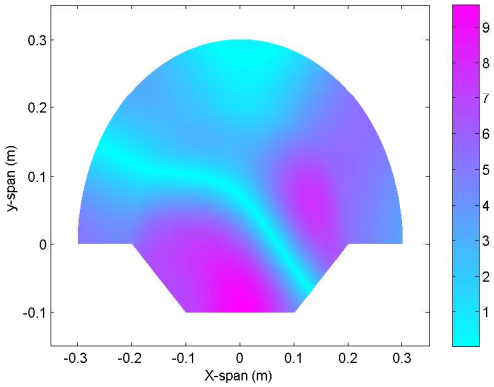

Figure 12: TE total field at $t=2.0LM$.

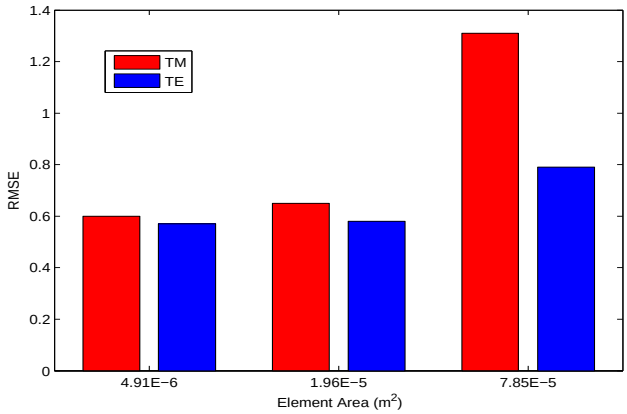

Figure 13: Time series root mean square error versus the average element area.

Figs. 11 and 12 are contour plots of the total field at a selected time, $t=2.0LM$, for TM and TE polarizations respectively. Note the strong traveling wave contribution that exists along the ground plane in the trough region for the TE^z case, as physically expected.

6 Error analysis

We examine the mesh-related error for the canonical geometry described in Section IV with a fixed time step, $\delta t = 0.01(LM)$. Analytical solutions for this case are given in Eqs. (4.7)-(4.10). At a fixed spatial point, the time series root mean square error (RMSE) is calculated as:

$$\mathrm{RMSE}(\Delta A) = \sqrt{\frac{1}{N}\sum_{i=1}^{N}[u_{num}(i)-u_{ana}(i)]^2}, \tag{6.1}$$

where ΔA is the average element area in the interior domain of the model, N the total number of time steps, $u_{num}(i)$ the numerically calculated total field at time step i, and $u_{ana}(i)$ the analytically calculated total field at time step i.

Fig. 13 depicts the relationship between RMSE and ΔA for both polarizations. It is noted that the TM^z error is somewhat more pronounced compared to that of the TE^z which is perfectly reasonable, resulting from different formulations.

7 Conclusion

We have implemented a hybrid method integrating the FEM algorithm and Laplace transform for solving the scattering of plane waves by overfilled cavities embedded in the 2D ground plane in the time domain. This formulation is developed to couple the interior and exterior fields on the overlapped domain. The analytical formulation has the desirable characteristic that it enables the optimal choice of the overlapped region such that a potentially time-consuming Schwartz iteration associated with conventional subdomain methods is avoided, hence drastically improving the efficiency of the algorithm.

In addition, the accuracy and reliability of our method are demonstrated both by the perfect linkage between the numerical solutions of the interior problem and those of the analytical over the exterior and the favorable comparison against the analytical solution for a canonical geometry.

Finally a time series error analysis is performed to investigate the relationship between the average mesh element area and root mean square error of the total field. This is helpful in determining the mesh refinement for a specified error tolerance.

Acknowledgments

This work was supported in part by the Air Force Office of Scientific Research. The views expressed in this article are those of the authors and do not reflect the official policy or position of the United States Air Force, Department of Defense, or the US Government.

References

[1] S. Lee, M. Vouvakis, and J. Lee, A non-overlapping domain decomposition method with non-matching grids for modeling large finite antenna arrays, J. Comput. Phys., vol. 203, no. 1, pp. 1-21, 2005.

[2] S. Gedney and U. Navsariwala, An unconditionally stable finite element time-domain solution of the vector wave equation, IEEE Microwave Guided Wave Lett. 5 (1995), pp. 332-334.

[3] F. Edelvik, G. Ledfelt, P. Lotstedt and D. Riley, An unconditionally stable subcell model for arbitrarily oriented thin wires in the FETD method, IEEE Trans. Antennas Propagat. 51 (2003) (8), pp. 1797-1805.

[4] D. White and M. Stowell, Full-wave simulation of electromagnetic coupling effects in RF and mixed-signal ICs using a time-domain finite-element method, IEEE Trans. Microwave Theory Tech. 52 (2004), pp. 1404-1413.
[5] D. Jiao, A. Ergin, B. Shanker, E. Michielssen and J. Jin, A fast time-domain higher-order finite-element-boundary-integral method for 3D electromagnetic scattering analysis, IEEE Trans. Antennas Propagat. 50 (2002) (9), pp. 1192-1202
[6] D. Jiao, J.M. Jin, E. Michielssen and D. Riley, Time-domain finite-element simulation of three-dimensional scattering and radiation problems using perfectly matched layers, IEEE Trans. Antennas Propagat. 51 (2003), pp. 296-305.
[7] D. Riley and J. Jin, Modeling of magnetic loss in the finite-element time-domain method, Microwave Opt. Tech. Lett. 46 (2005) (2), pp. 165-168.
[8] Z. Lou and J. Jin, An accurate waveguide port boundary condition for the time-domain finite element method, IEEE Trans. Microwave Theory Tech. 53 (2005), pp. 3014-3023.
[9] Z. Lou and J. Jin, Modeling and simulation of broadband antennas using the time-domain finite element method, IEEE Trans. Antennas Propagat. 53 (2005), pp. 4099-4110.
[10] T. Van and A. W. Wood, A time-marching finite element method for an electromagnetic scattering problem, Math. Methods in the App. Sciences, Vol. 26 (2003), pp.1025-1045.
[11] T. Van and A. W. Wood, A time-domain finite element method for Helmholtz equations, J. Comp. Physics, Vol. 183 (2002), pp. 486-507.
[12] T. Van and A. W. Wood, Analysis of transient electromagnetic scattering from over-filled cavities, SIAM J. App. Math, Vol. 64, No. 2 (2004), pp. 688-708.
[13] T. Van and A. W. Wood, A time-domain finite element method for Maxwell's equations, SIAM J. Num. Anal., Vol. 42, No. 4 (2004), pp. 1592-1609.
[14] T. Van and A. W. Wood, Finite element analysis of transient electromagnetic scattering from 2d cavities, Methods and Applications of Analysis, Vol. 11, No. 2 (2004), pp. 221-236.
[15] T. Van and A. W. Wood, Finite element analysis of transient electromagnetic scattering problems, Adv. Comp. Math., Vol. 22, No. 1 (2005), pp. 21-48.
[16] B. H. Jung, T. K. Sarkar, Y. S. Chung, M. Salazar-Palma, Z. Li, S. Jang, and K. Kim, Transient electromagnetic scattering from dielectric objects using the electric field integral equation with Laguerre polynomials as temporal basis functions, IEEE Trans. Antennas Propagat. 52 (2004) (9), pp. 2329-2340.
[17] H. Vollmer and E. Rothwell, Resonance series representation of the early-time field scattered by a coated cylinder, IEEE Trans. Antennas Propagat. 52 (2004) (8), pp. 2086-2190.
[18] Z. Luo and J. Jin, A dual-field domain-decomposition method for the time-domain finite-element analysis of large finite arrays, J. Comput. Phys. 222 (2007), pp. 408-427.
[19] C. Farhat, A method of finite element tearing and interconnecting and its parallel solution algorithm, Int. J. Numer. Method. Eng. 32 (1991) (6), pp. 1205-1227.
[20] C. Farhat, N. Maman and G. Brown, Mesh partitioning for implicit computations via iterative domain decomposition: impact and optimization of the subdomain aspect ratio, Int. J. Numer. Method. Eng. 38 (1995) (6), pp. 989-1000.
[21] H. A. Schwartz, Gesammelete Mathematische Abhandlungen, vol. 2, Springer, Berlin, pp. 133-143, 1890.
[22] J. Huang and A. Wood, Numerical Simulation of Electromagnetic Scattering Induced by an Overfiled Cavity in the Ground plane, IEEE Antennas and Wireless Propagation Letters, 4 (2005), pp. 224-228.
[23] C. W. Wu, L. C. Kempel, S. w. Schneider, and K. D. Trott, Hybrid finite element-boundary integral method for cavities recessed in an elliptic cylinder; IEEE Trans. Antennas Propagat.

51 (2003) (8), pp. 1829 - 1836.
[24] C. A. Macon, L. C. Kempel, S. w. Schneider, and K. D. Trott, Modeling conformal antennas on metallic prolate spheroid surfaces using a hybrid finite element method, IEEE Trans. Antennas Propagat. 52 (2004) (3), pp.750 - 758
[25] A. W. Wood, Analysis of electromagnetic scattering from an over-filled cavity in the ground plane, J. Comput. Phys., vol.215, pp.630-641 (2006).
[26] H. Ammari, G. Bao and A. Wood, A cavity problem for Maxwell's equations, J. Meth. Math. Appl., vol.9, pp.249-260, 2002.
[27] H. Ammari, G. Bao and A. Wood, An integral equation method for the electromagnetic scattering from cavities, J. Math. Meth. Appl. Sci., vol. 23, pp. 1057-1072, 2000.
[28] H. Ammari, G. Bao and A. Wood, Analysis of the electromagnetic scattering from a cavity, Japan J. Indus. Appl. Math., vol.19, pp.301-308, 2001.
[29] J. Huang and A. Wood, Analytical and Numerical solution of Transient Electromagnetic Scattering from Overfiled Cavities, Commun. Comput. Phys., 1 (6) (2006), pp. 1043-1055.
[30] K. S. Crump, Numerical inversion of Laplace transforms using a Fourier series approximation, Journal of the Association for Computing Machinery, 23, pp. 89-96, 1976.
[31] F. R. de Hoog, J.H. Knight, and A.N. Stokes, An improved method for numerical inversion of Laplace transforms, SIAM J. Sci. Stat. Comput., 3, pp. 357-366, 1982.
[32] D. E. Amos, A Subroutine Package for Bessel Functions of a Complex Argument and Nonnegative Order, Sandia National Laboratory Report, SAND85-1018, May, 1985.
[33] D. E. Amos, A Portable Package for Bessel Functions of a Complex Argument and Nonnegative Order, Trans. Math. Software, 1986.
[34] J.M. Jin, The Finite Element Method in Electromagnetics, second ed., pp. 539-540, Wiley, New York, 2002.
[35] K. J. Hollenbeck, (1998) INVLAP.M: A MATLAB function for numerical inversion of Laplace transforms by the de Hoog algorithm.
`http://www.mathworks.com/support/ solutions/files/s1-1AYAE/invlap.m`